Directional Mass Transport by Momentum Transfer from Ion Beam to Solid

L. Cliche,[1] S. Roorda,[1] M. Chicoine,[1] and R. A. Masut[2]

[1]*Département de Physique, Université de Montréal, C.P. 6128, succ. centre-ville, Montréal, Quebec, Canada H3C 3J7*

[2]*Départment de Génie Physique, École Polytechnique de Montréal, C.P. 6079, succ. centre-ville, Montréal, Quebec, Canada H3C 3A7*

(Received 28 November 1994)

Irradiation of InP with MeV Se ions directed a few degrees off the surface normal leads to a lateral displacement of the implanted material. Adjacent surface regions that are not irradiated remain unaffected. The dependence of the displacement on ion energy and its directionality strongly suggest that the effect is caused by momentum transfer from the ion to the solid. The amount of displaced material as a function of ion beam energy or angle of incidence can be described with a simple model incorporating a shear stress, applied to the target as the ion slows down, and radiation enhanced viscosity.

PACS numbers: 61.80.Jh, 68.55.Ln, 79.20.Nc

When an energetic ion penetrates a solid it is decelerated via two different processes: elastic collisions with target nuclei and electronic excitation of target atoms. Both processes are regarded normally as energy loss processes, and for an evaluation of macroscopic consequences of ion irradiation the momentum of the incident ion is not considered. For example, a method for estimating the number of displaced atoms generated by the ion is to evaluate the rate of energy loss into elastic collisions [1]. Some results have been reported which indicate that energy loss may not be the full story, and that the ion momentum has to be considered as well. In the case of a high fluence, high flux, and high temperature keV As implantation into Si, the material became porous near the surface, whereas deeper layers contained dislocation loops [2]. This defect structure suggested that *microscopic* momentum transfer from the ion to target atoms during elastic collisions resulted in a spatial separation of vacancies and interstitials, with the vacancies remaining near the surface and the interstitials kicked into deeper regions. An observation of a different nature is that during ion irradiation of amorphous metal alloys, at several hundred MeV, thin films become larger but thinner, as if the films were between a hammer and anvil [3]. It has been explained in terms of Coulomb explosions in the wake of the ions. This explanation has met with some controversy, since Coulomb explosions are more likely to occur in insulators than in conductors.

In this Letter we present experimental observations that are strongly suggestive of *macroscopic* momentum transfer effects. Patches of InP were found to be displaced laterally following off-normal, MeV ion implantation. The displacement is orders of magnitude larger than the vacancy-interstitial separation observed as a result of microscopic momentum transfer. The energy dependence of the process shows that the momentum transfer occurs along the entire ion track, i.e., not only in the elastic collision but also in the electronic excitation regime.

Semi-insulating InP(100) wafers were clamped to a copper block using a thin layer of conductive paste for good thermal contact. Some samples were uniformly implanted with 10^{14} cm^{-2} Se ions at several energies (2, 3.6, 6, 10, 17, 24, 30, and 35 MeV) in order to produce thick (~ 8 μm) uniform amorphous layers. Raman spectroscopy was used to verify that the near surface of InP is indeed amorphous after 2 MeV, 10^{14} cm^{-2} Se implantation. All samples were then implanted through a steel contact mask in order to produce alternating implanted and nonimplanted regions. All the implantations were conducted at -180 °C. The implanted surfaces were characterized with a stylus profilometer (Dektak 3030ST).

Figure 1 shows the surface profile of a *c*-InP substrate which had been implanted with 30 MeV Se ions at a fluence of 10^{15} atoms/cm^2. The angle between ion beam and surface normal was 7°, with an orientation as indicated on the figure. We notice two important modifications of the implanted regions as compared to those covered by the mask. First, there is an overall depression of each implanted surface of about 0.1 μm. We attribute this to a compaction of the bombarded material. Such a depression is expected since it has

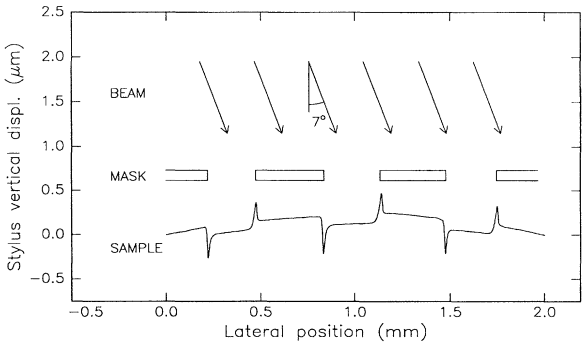

FIG. 1. Surface profile of a *c*-InP substrate implanted through a contact mask with 30 MeV, 10^{15} Se/cm^2 at 7° off normal.

 0031-9007/95/75(12)/2348(4)$06.00

already been established [4] that in its relaxed state, amorphous InP is 0.17% more dense than c-InP. Second and most striking, we see a valley shape on the left side of each implanted region with a corresponding peak shape on the opposite side. In a three-dimensional description, the valley and peak shape are indicative of a ditch and a dike structure, respectively. The in-plane component of the ion's momentum was always pointing from the ditch structure to the dike structure. Because surface profiles scanned in the opposite direction (from right to left) were found to be identical to the ones shown, we conclude that this effect was not due to an overshoot or undershoot of the profilometer stylus.

Figure 2 shows scanning electron microscopy (SEM) pictures of the same sample after it was cleaved along the Dektak trace. Figure 2(a) shows a plan view of the left edge of an implanted region while Fig. 2(b) shows the cross-sectional view. Figures 2(c) and 2(d) are the same views of the corresponding right side of an implanted region. The two regions depicted by the SEM pictures are indicated by rectangular boxes on the surface profiles at the bottom of Fig. 2, where the structures clearly stand out due to the magnified y-axis scale. Even though it is more difficult to see the vertical displacement of the surface on the SEM pictures, it is nevertheless possible to identify the ditch and dike structures by looking at the cleaved edge. Moreover, the SEM images show that the structures are smooth, and that they can be easily profiled by the stylus of the profilometer.

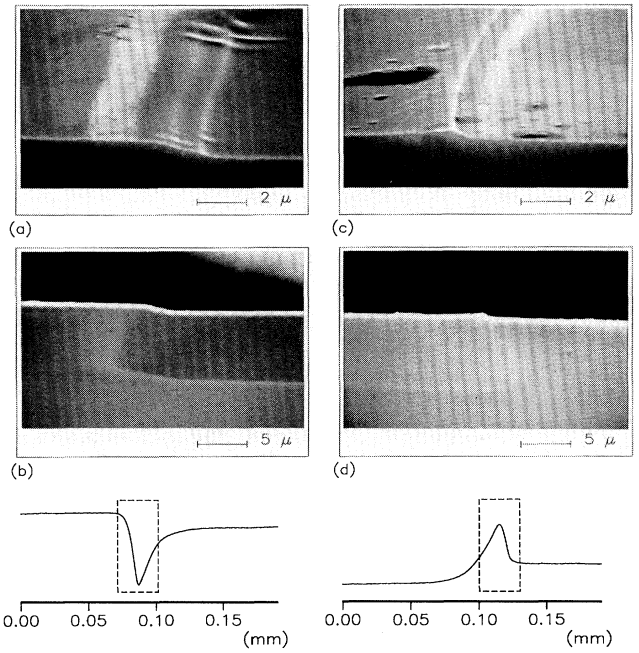

FIG. 2. SEM pictures of (a) a plan view and (b) cross-sectional view of the left edge of an implanted region for the same sample presented in Fig. 1. (c),(d) The same views of the corresponding right side of an implanted region. The two regions depicted in (b) and (d) are indicated by rectangular boxes on the surface profiles at the bottom.

The location of the ditch and dike structures in relation to the direction of the lateral component of the initial ion momentum strongly suggests that the latter plays an important role in the creation of the former. Another clue is provided by the size of the dike: A stretch of 1 cm of the dike contains about 1.5×10^{15} atoms, adjacent to a 0.3 mm wide strip that received 3×10^{13} ions during the ion implantation. If the dike was caused by microscopic momentum transfer during elastic collisions, each incident ion would have to displace 50 recoils over 300 μm (or 15 000 recoils over 1 μm, or equivalent). Since only the lateral component of the ion momentum is involved, this seems unlikely if not physically impossible. We therefore suggest another mechanism: macroscopic momentum transfer along the entire ion track. Before discussing this mechanism in detail, it should be mentioned that other possibilities exist for the generation of the dike structure, one such possibility is sputtering and deposition of the (steel) mask. This explanation can be excluded for two reasons. First, energy dispersive x-ray (EDX) analysis of the dike structure showed no measurable traces of Fe or Ni on the InP surface and, second, sputter erosion of the mask, even though it may lead to the formation of a dike, cannot explain the formation of the corresponding ditch structure.

At this point, it may be mentioned that the size of the ditch and dike did not depend on ion flux (from 10 to 115 nA/cm^2) and increased linearly with ion fluence (from 5×10^{13} to 1×10^{15} atoms/cm^2). Cooling during the irradiation proved essential: The ditches and dikes are only observed after liquid nitrogen cooled irradiations and are completely absent after room temperature irradiation.

We propose the following scenario for mass transport by momentum transfer. It consists essentially of two parts. First, the ion exerts a force on the solid as it slows down and, second, the solid responds and deforms. The force exerted on the target is obviously the exact opposite of the force acting on the ion. This force is present regardless of the atomic mechanism responsible for slowing down the ion. In the case of electronic excitation, the excited electrons carry momentum in all directions, but with a net momentum equal to that lost by the ion. As the excited electrons interact with the target nuclei, the momentum *must be* transferred to the target.

If the target is really solid, it will simply transfer the momentum to the environment with no further permanent change to the target. However, the target is deformable: It has been observed experimentally [5] that, during MeV ion irradiation, strain can be relieved by viscous flow and it has been established theoretically [6] that, during a few ps after a keV collision cascade, a small region around the ion track melts (this theoretical result concerns melting in the nuclear stopping regime; here we tentatively extend it to the electronic stopping regime, i.e., along the entire ion track). Since, in the target shown in Figs. 1 and 2,

a component of the force acting on the target was in the plane of the surface, the response of the short-lived liquid is to move sideways relative to the surrounding solid. We surmise that it freezes in the deformed state. The cumulative effect of a sequence of ion impacts is a lateral displacement of the entire surface layer. It may be added here that in the absence of liquidlike cascade effects the target is still deformable, because point defects such as broken bonds created by the incident ions lead to radiation-enhanced flow in amorphous materials. However, this effect is not expected to play a significant role in the present situation because the force is applied to the target only during the short time the ion is slowed down.

In Fig. 3 we have compared the amount of mass transport as a function of initial ion energy with the amount predicted by a simple model based on the scenario described above. The points are the experimentally determined amounts of mass flow as it occurred in preamorphized InP that had been implanted (at 77 K and 7° off normal) with 3×10^{14} Se/cm^2 at several energies. The amount of displaced material was determined as the average value of the missing atoms in the volume of 1 cm of the ditch structure and the extra atoms in 1 cm of the dike structure. Each point (error) is the average value (variance) of six individual structures. It can be seen that the amount of displaced material increases superlinearly with incident ion energy. The lines correspond to estimates of the amount of displaced material based on the scenario described above and according to different possible relations between the local ion energy loss and target deformability.

The relation between the lateral shear stress τ_{lat} applied to a viscous medium and the resulting lateral displacement velocity v_{lat} can be expressed as follows:

$$\tau_{\text{lat}} = -\eta \frac{\Delta v_{\text{lat}}}{\Delta y} = -\eta \frac{\partial v_{\text{lat}}}{\partial_y}, \qquad (1)$$

where η is the viscosity of the material and y the depth beneath the surface. In applying this expression, we have deduced the stress and viscosity from the ion

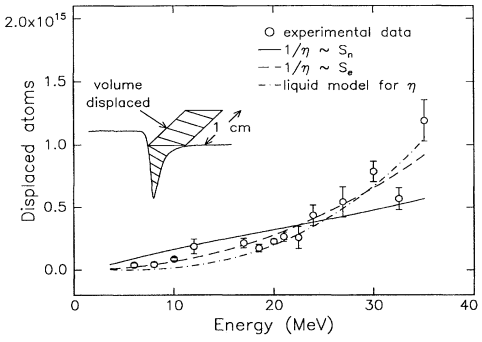

FIG. 3. Number of atoms along 1 cm, displaced by 3×10^{14} Se/cm^2 as a function of initial ion energy. Also shown are the estimates of the total mass transport using a viscosity inversely proportional to S_n (solid line), S_e (dashed line), and with a liquidlike behavior viscosity (dashed-dotted line).

energy loss along its track, and integrated it numerically to obtain a measure for the lateral velocity during a cascade. Multiplied by the time duration of a cascade and by the implantation fluence, it gives an estimate of the total mass transport. The lateral stress at depth y was deduced from the ion energy loss dE/dr according to

$$\tau_{\text{lat}} = -\frac{\sin\theta}{A} \frac{dE}{dr}, \qquad (2)$$

where θ is the incident angle between ion beam and surface normal, and A is the surface area of the ion track. The viscosity was estimated in three different ways, corresponding with the three curves shown in Fig. 3. The first two methods assume that the target remains essentially solid, but that point defects such as broken bonds mediate flow, whereas the third method assumes that a small region around the ion track is liquid for a period of a few ps.

If the viscosity is dominated by flow defects introduced by the ion beam (i.e., at relatively high viscosities and low defect densities), $1/\eta$ is proportional to the defect density [7]. If the viscosity is dominated by vacancies and interstitials, $1/\eta$ would be proportional to the nuclear energy loss, S_n, and if broken or dangling bonds dominate, it would be proportional to the electronic energy loss, S_e. These options correspond to the dashed and solid lines in Fig. 3, respectively. However, the defect model of η may not be applicable in our case. If the ion track is indeed liquid, the behavior of the viscosity along it will be dominated by its temperature dependence instead of the defect density. To implement this, we have assumed that the total energy lost by the ion is distributed among the atoms in a 10 nm cylinder surrounding the ion trajectory. The resulting energy per atom was used as the temperature at which the thermally activated viscosity was calculated. The result of numerically integrating the velocity profiles thus obtained is plotted in Fig. 3 as a dashed-dotted line. In all three cases, well-established values for the energy loss along the ion track were used [8]. It should be added that none of the three models take into account spatial or temporal variations in defect densities or temperature other than finite size and duration of the ion tracks.

Comparing the curves in Fig. 3 with the data points, it can be seen that the latter two models describe the data reasonably well. They have in common that, as the ion energy increases, the near-surface region becomes increasingly less viscous. On the basis of a cascade duration of 1 ps and a track radius of 10 nm which would imply that 2.4×10^7 atoms are displaced by 6 Å for each individual ion, the amount of mass transport per ion requires a viscosity varying from 1 to 10^3 P. This viscosity is unphysically low for a solid where flow is mediated by broken bonds and is closer to that of a real liquid; it would confirm that cascade regions can behave like a liquid. More importantly, the fact that the occurrence and energy dependence of the observed

structures can be described qualitatively and quantitatively with such a simple model shows that the most likely cause is indeed directional mass transport by momentum transfer from the ion to the target.

The validity of the momentum transfer mechanism is even more convincingly demonstrated by the angular dependence of the mass transport. We have measured the amount of mass transport as a function of incident angle θ, and the results are shown in Fig. 4. According to the scenario sketched above, a $\sin\theta\cos\theta$ type behavior is expected, since the shear stress increases as $\sin\theta$ whereas the penetration depth decreases as $\cos\theta$. The curve in Fig. 4 is a best fit of a $\sin\theta\cos\theta$ function to the data points, and it is seen to describe the data well. This not only confirms the validity of the momentum transfer mechanism but also rules out (again) the possibility of sputtering or deposition from the beam defining mask.

An alternative explanation for these data can be proposed, involving the interplay of sputtering and surface diffusion. On one side of the mask, some of the ions pass through the edge of the mask and then hit the InP surface with an energy of ~110 keV instead of 30 MeV. This will lead to enhanced sputtering (the sputtering yields at 30 MeV and 110 keV are 1.4 and 15, respectively [9]). If the sputtered atoms remain on the surface, diffuse, and accumulate at the other side of the mask, this would lead to the structures observed in Fig. 1. However, the observed ditch is 0.3 μm deep, whereas the maximum erosion, after 10^{15} ions/cm^2 at the maximum sputter yield, is only 40 Å. Moreover, the surface diffusion would be more effective at room temperature than at liquid nitrogen temperature [10] which is exactly opposite to the observed behavior.

A few remarks are in order. First, the effect is not restricted to the combination of Se ions and InP targets; with other combinations we have observed comparable effects. Second, an alternative explanation for the Klaumünzer effect can now be formulated. For normal incidence, the liquid material in the cascade region experiences a downward force directed along the surface normal. Inertia of the underlying substrate converts that force to a compressive stress, to which the cascade region would respond by becoming wider and thinner. In other words, the combination of fast ion and solid substrate really acts as a hammer and anvil, between which the surface layers are sandwiched.

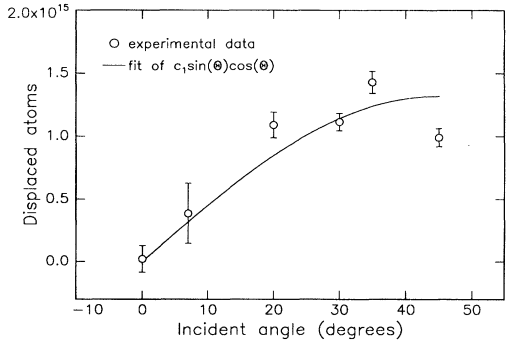

FIG. 4. Number of displaced atoms along 1 cm as a function of angle θ between ion beam and surface normal. Samples were implanted with 24 MeV, 3×10^{14} Se/cm^2.

In conclusion, we have discovered a new phenomenon in beam-solid interaction, namely, momentum transfer induced mass transport. The effect becomes prominent during heavy ion irradiation with ion energies exceeding a few MeV, and appears to be mediated most effectively by electronic excitation of the target. The dependence of the amount of mass transport on the incident ion energy has been successfully described by numerically integrating the depth profile of the lateral displacement velocity, which in turn was calculated from the force applied to the target by the slowing of the ion, and the estimated viscosity along the ion track.

The authors thank F. Spaepen and C. A. Volkert for helpful discussions. Thanks are due to P. Bérichon and R. Gosselin for their expert assistance during the irradiation experiments. We also thank M. Caron for performing SEM and EDX analysis. This work is financially supported by the Natural Sciences and Engineering Research Council of Canada (NSERC) and the Fonds pour las Formation de Chercheurs et l'Aide à la Recherche (FCAR).

Note added.—After we submitted our manuscript, a Letter was published concerning beam-induced macroscopic deformation of glassy metals [11]. We strongly suspect that the momentum transfer driven mechanism put forward in the present work plays a decisive role in generating those deformations.

[1] G. H. Kinchin and R. S. Pease, Rep. Prog. Phys. **18**, 1 (1955).
[2] O. W. Holland and C. W. White, Nucl. Instrum. Methods Phys. Res., Sect. B **59/60**, 353 (1991).
[3] S. Klaumünzer and G. Schumacher, Phys. Rev. Lett. **51**, 1987 (1983); S. Klaumünzer, Ming-dong Hou, and G. Schumacher, Phys. Rev. Lett. **57**, 850 (1986).
[4] L. Cliche, S. Roorda, and R. A. Masut, Appl. Phys. Lett. **65**, 1754 (1994).
[5] C. A. Volkert, J. Appl. Phys. **70**, 3521 (1991).
[6] T. Diaz de la Rubia and G. H. Gilmer, Phys. Rev. Lett. **74**, 2507 (1995).
[7] A. Witvrouw and F. Spaepen, J. Appl. Phys. **74**, 7154 (1993).
[8] J. F. Ziegler, J. P. Biersack, and U. Littmark, *The Stopping and Ranges of Ions in Matter* (Pergamon, New York, 1985), Vol. 1.
[9] P. Matsunami *et al.*, At. Data Nucl. Data Tables **31**, 1 (1984).
[10] E. Chason, T. M. Mayer, B. K. Kellerman, D. T. McIlroy, and A. J. Howard, Phys. Rev. Lett. **72**, 3040 (1994).
[11] A. Gutzmann, S. Klaumünzer, and P. Meier, Phys. Rev. Lett. **74**, 2256 (1995).

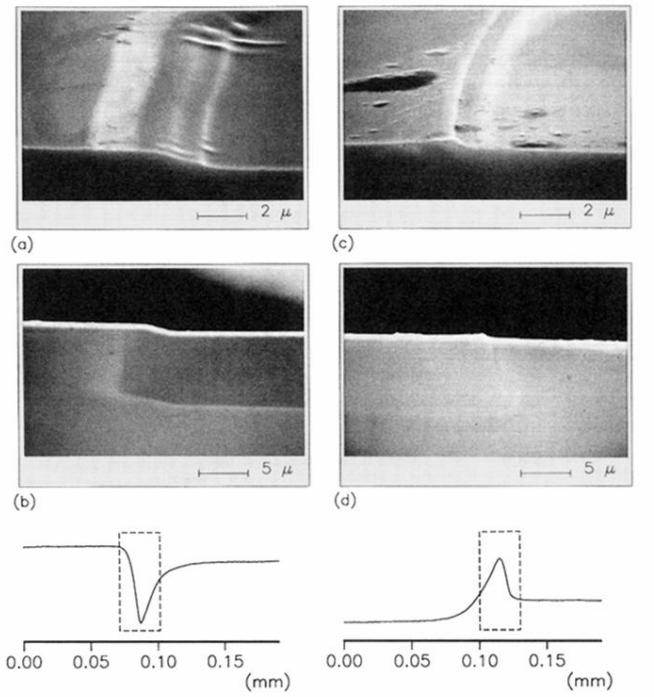

FIG. 2. SEM pictures of (a) a plan view and (b) cross-sectional view of the left edge of an implanted region for the same sample presented in Fig. 1. (c),(d) The same views of the corresponding right side of an implanted region. The two regions depicted in (b) and (d) are indicated by rectangular boxes on the surface profiles at the bottom.